ES Energy & Environment
DOI : https://dx.doi.org/10.30919/esee8c521

Non-Monotonic Thickness Dependent Hydrodynamic Phonon Transport in Layered Titanium Trisulphide: First-Principles Calculation and Improved Callaway Model Fitting

Chenhan Liu,[1,*] Chao Wu,[2] Ping Lu[1] and Yunshan Zhao[3,*]

Abstract

Different from diffusive and ballistic phonon transport, the hydrodynamic phonon transport has many unique thermal properties such as super-linearity dependence of thermal conductivity on width and macroscopic phonon motion. In this work, the thickness dependent hydrodynamic phonon transport in layered titanium trisulphide (TiS_3) is investigated by first-principles calculation and improved Callaway model. From the picture of linearized phonon Boltzmann transport based on first-principles calculation, two indicators at 100 K clearly show the existence of hydrodynamic phonon transport: the displaced phonon distribution with a constant drift velocity regardless of phonon wavevector and phonon polarization as well as the much larger N scattering rates than U scattering rates. The extracted drift velocity decreases significantly from 1954 m/s to 241 m/s under a temperature gradient 10^7 K/m as the temperature increases from 50 K to 100 K. From the improved Callaway model, the hydrodynamic phonon transport has a non-monotonic dependence on thickness due to the competition between phonon-phonon scattering and phonon-boundary scattering. The non-monotonic dependence can better understand the phonon properties of hydrodynamic transport and help design materials to observe hydrodynamic phonon transport experimentally. The temperature, width and length effects on the phonon transport behavior are also discussed individually.

Keywords: Hydrodynamic phonon transport; Layered material; First-principles calculation.
Received: 1 August 2021; Accepted: 1 September 2021.
Article type: Research article.

1. Introduction

Phonons, as one kind of fundamental energy carriers, determine the thermal properties of nonmetals including semiconductors and insulators. In the Boltzmann-Peierls picture,[1] phonons suffer from a series of scattering events with crystal impurities, boundaries or other phonons along their transport trajectories. From the thermal resistance point of view, only phonon-phonon scattering events with conserved momentum are non-resistive (N process); while all other scattering events can be treated as resistive (R process).[2] At the macroscopic scale, R process is dominant and phonon transport is diffusive. While at the nanometer scale such as the feature size of transistor in the integrated circuit down to few nanometers, the phonon transport becomes ballistic. Between these two different scales, a new phonon transport phenomenon (different from diffusive and ballistic transport) called hydrodynamic have been theoretically and experimentally explored.[2-10] Such transport phenomenon, typically sandwiched between diffusive and ballistic regimes,[8,9] has many unique properties such as superliner width dependent thermal conductivity and macroscopic motion of phonons.[3] Compared to the diffusive transport, the hydrodynamic transport has no thermal resistance; while compared to the ballistic transport, the hydrodynamic transport can transport much longer distance before losing collective property.[11,12] Therefore, to investigate hydrodynamic phonon transport phenomenon is important and

[1] *Engineering Laboratory for Energy System Process Conversion & Emission Reduction Technology of Jiangsu Province, School of Energy and Mechanical Engineering, Nanjing Normal University, Nanjing, 210046, China.*
[2] *Jiangsu Key Laboratory for Design and Manufacture of Micro-Nano Biomedical Instruments, School of Mechanical Engineering, Southeast University, Nanjing, 211100, China.*
[3] *NNU-SULI Thermal Energy Research Center (NSTER) & Center for Quantum Transport and Thermal Energy Science (CQTES), School of Physics and Technology, Nanjing Normal University, Nanjing 210023, China.*
**Email:* phyzys@njnu.edu.cn (Zhao), chenhanliu@njnu.edu.cn (C. Liu)

necessary.

The hydrodynamic phonon transport is the collective motion of phonons and the term "collective" means that the flux of phonons can be represented by a single value of macroscopic drift velocity regardless of their wave vectors and frequencies.[3] In order to observe the hydrodynamic transport, N process of phonon scattering events should be strong while R process become weakened simultaneously. Typically decreasing temperature to suppress R process is an efficient method to observe the hydrodynamic phonon transport. However, if the temperature is too low, the transport becomes ballistic easily due to the lack of enough N scattering events, leading to a quite narrow temperature range for hydrodynamic transport. This is perhaps the reason why the studies on this topic have been inactive even there exists experimental studies several decades ago.[13,14] Thus, for hydrodynamic phonon transport to be dominant, two conditions should be satisfied at the same time in order to guarantee strong N process and weak R process during phonon transport: high Debye temperature and strong anharmonicity.[12]

In graphitic materials such as graphene and single-wall carbon nanotube, the first condition of high Debye temperature is satisfied due to the strong bond and low mass of carbon. In addition, ZA modes are the main contributors to heat transport and are strongly anharmonic for small wavevector states,[15] satisfying the second condition of strong anharmonicity as well. Thus, several theoretical studies observed the distinct hydrodynamic phonon transport in those graphitic materials by first-principles calculations.[3,4,6] Recently the hydrodynamic phonon transport was experimentally observed in graphite thin film by using a standard steady-state one-heater-two-thermometers technique.[8] Moreover, the second sound, which is another indictor of strong N process during phonon transport, was also clearly observed in graphite by using time-resolved optical measurements.[7] Among those works, some observed distinct hydrodynamic phonon transport while others not. For example, compared to that of bulk graphite, monolayer graphene has a more obvious hydrodynamic transport behavior,[3,4] *i.e.* the hydrodynamic transport in monolayer graphene occurs within a larger temperature range and larger width range. The reason is due to the lack of interlayer phonon coupling, which is resistive since the interlayer coupling due to the increase of thickness can decrease the thermal conductivity.[11] However, how the thickness affects the hydrodynamic transport is not investigated up to now. As indicated in Refs. 16-18, the in-plane thermal conductivity has a non-monotonic dependence on thickness in two-dimensional layered materials. Whether the dependence of hydrodynamic phonon transport on thickness is non-monotonic with a similar way is unclear. Apart from the graphitic materials, there is lacking of studies on whether other layered materials have hydrodynamic phonon transport as well.

In order to investigate the hydrodynamic phonon transport, several different theoretical methods including first-principles calculation,[3] Monte Carlo simulation,[9] improved Callaway fitting,[19] kinetic-collective model[5] and Guyer and Krumhansl equation[20-22] have been employed. In this work, the first-principles calculation and improved Callaway model are adopted considering their advantages in separating N and U scattering processes. The first-principles calculation can obtain the displaced phonon distribution as well as the different U and N scattering rates. The improved Callaway model can determine the individual contribution of N and U scatterings to the thermal conductivity. The parameters in the improved Callaway model are fitted based on the temperature dependent thermal conductivity from the first-principles calculation. The layered material TiS_3 is chosen to investigate the hydrodynamic phonon transport, considering their potential applications such as in field effect transistors[23] and electrode materials[24-26] for rechargeable Li and Na ion batteries.

2. Model and Methods

In this work, Phonopy package[27] is applied to calculate phonon properties and Sheng BTE package[28] is applied to calculate phonon scattering information. The relaxed structure, second-order and third-order force constants needed by the two packages are calculated by using the Vienna Ab-initio Simulation Package (VASP). The detailed parameters setting during the calculation can be found in Ref.[18]

For the first-principles calculation, the linearized Boltzmann transport equation is applied to describe the phonon transport and the in-plane thermal conductivity of TiS_3 k can be calculated as following:[28-30]

$$k_{\alpha\beta} = \frac{1}{k_B T^2 \Omega n} \sum_\lambda f_0 (f_0 + 1) (\hbar\omega)^2 v_\lambda^\alpha v_\lambda^\beta \tau_\lambda \quad (1)$$

$$\frac{1}{\tau_\lambda} = \frac{1}{n} \left(\sum^+_{\lambda' \lambda''} \Gamma^+_{\lambda\lambda'\lambda''} + \frac{1}{2} \sum^-_{\lambda' \lambda''} \Gamma^-_{\lambda\lambda'\lambda''} + \sum_{\lambda'} \Gamma_{\lambda\lambda'} \right) \quad (2)$$

$$\Gamma^+_{\lambda\lambda'\lambda''} = \frac{\hbar\pi (f_0' - f_0'')}{4\omega_\lambda \omega_{\lambda'} \omega_{\lambda''}} \left| V^+_{\lambda\lambda'\lambda''} \right|^2 \delta(\omega_\lambda + \omega_{\lambda'} - \omega_{\lambda''}) \quad (3)$$

$$\Gamma^-_{\lambda\lambda'\lambda''} = \frac{\hbar\pi (f_0' + f_0'' + 1)}{4\omega_\lambda \omega_{\lambda'} \omega_{\lambda''}} \left| V^-_{\lambda\lambda'\lambda''} \right|^2 \delta(\omega_\lambda - \omega_{\lambda'} - \omega_{\lambda''}) \quad (4)$$

where α (β) denotes the direction x (a axis of TiS_3 unit cell) or y (b axis), T is the temperature, k_B is the Boltzmann constant, n is the number of phonon modes λ including phonon wavevector q and phonon polarization, Ω is the volume of unit cell, f_0 is the equilibrium phonon (Bose-Einstein) distribution, $\hbar$ is the reduced Planck constant, v is the phonon group velocity, ω is the phonon angular frequency, τ is phonon lifetime (inverse of phonon scattering rates) and V is the scattering matrix element.[31,32] The phonon-phonon scattering process can be divided into adsorption process $\Gamma^+_{\lambda\lambda'\lambda''}$ (two incident phonons merge into one phonon) and emission process $\Gamma^-_{\lambda\lambda'\lambda''}$ (one phonon splits into two phonons). For both adsorption and emission processes, the energy conservation indicated by the Dirac delta function in Equations (3) and (4) should be satisfied. However, the phonon momentum during the scattering process can have a difference of reciprocal lattice vector. If phonon momentum is conserved in the three-phonon process ($q_{\lambda''} = q \pm q_{\lambda'}$), the scattering process is N

(Figs. 1(a) and (c)), while if phonon momentum has a difference of reciprocal lattice vector G ($q_{\lambda''} = q \pm q_{\lambda'} + G$), the scattering process is U (Figs. 1(b) and (d)). For the hydrodynamic transport to be dominant, the N scattering rates should be much larger than U scattering rates, as indicated in the graphene[3] and graphite.[4]

Another indicator of the hydrodynamic phonon transport can be found through the displaced phonon distribution. If R scattering is weak and can be ignored among the phonon transport process, the displaced phonon (Bose-Einstein) distribution can be written as:[3,33]

$$f_\lambda = \left(exp\left(\frac{\hbar(\omega - q\cdot u)}{k_B T}\right) - 1\right)^{-1} \quad (5)$$

The displacement u represents the drift velocity. In the displaced distribution, the drift velocity is a constant regardless of phonon wavevector and phonon polarization, similar to that of macroscopic transport phenomena in fluid. Assuming a small drift velocity, the displaced distribution can be simplified as following:

$$f_\lambda = f_0 + \frac{\hbar}{k_B T} f_0(f_0 + 1) q \cdot u \quad (6)$$

Correspondingly, the normalized deviation of phonon distribution $\bar{f}' = \frac{(f_\lambda - f_0)}{f_0(f_0+1)}$ is $\frac{\hbar}{k_B T} q \cdot u$ following the definition in Ref.[3]. Thus, if $\bar{f}'$ has a linear dependence on phonon wavevector, there exists the macroscopic motion of phonon transport and the slope of this dependence means the value of constant drift velocity of the macroscopic motion. In order to calculate $\bar{f}'$, we adopt formulas from Ref.[28] In a small temperature gradient, the phonon distribution f_λ can be calculated as following as well:

$$f_\lambda = f_0 + g_\lambda = f_0 - \vec{F} \cdot \overrightarrow{\nabla T} \frac{df_0}{dT} \quad (7)$$

$$\frac{df_0}{dT} = f_0(f_0 + 1) \frac{\hbar\omega}{k_B T^2} \quad (8)$$

where g_λ is equal to $-\vec{F} \cdot \overrightarrow{\nabla T} \frac{df_0}{dT}$, and $\vec{F}$, with the dimension of length, has the information of phonon mean free path. With the help of equation (8), $\bar{f}'$ is calculated:

$$\bar{f}' = \frac{(f_\lambda - f_0)}{f_0(f_0+1)} = -\vec{F} \cdot \overrightarrow{\nabla T} \frac{\hbar\omega}{k_B T^2} \quad (9)$$

In Equation (9), $\vec{F}$ can be obtained directly from ShengBTE package.

In this work, the improved Callaway model[19] is also applied to investigate the hydrodynamic phonon transport. Based on the model, the thermal conductivity k_{total} has two items:

$$k_{total} = K_C + K_N \quad (10)$$

where K_C is the Debye term, describing the resistive process and is given by

$$K_C = \frac{1}{\Omega n} \sum_\lambda \hbar\omega_\lambda v_{\lambda x}^2 \tau_\lambda^C \, \partial f_0 / \partial T \quad (11)$$

K_N is the N-drift term, describing the non-resistive process and is given by

$$K_N = k_1 / k_2 k_3 \quad (12)$$

$$k_1 = \frac{1}{\Omega n} \sum_\lambda v_{\lambda x} \lambda_x \tau_\lambda^C \, \partial f_0 / \partial T \quad (13)$$

$$k_2 = \frac{1}{\Omega n} \sum_\lambda v_{\lambda x} \lambda_x \left(\tau_\lambda^C / \tau_\lambda^N\right) \partial f_0 / \partial T \quad (14)$$

$$k_3 = \frac{1}{\Omega n} \sum_\lambda (\lambda_x^2 / \hbar\omega_\lambda) \left(\tau_\lambda^C / \tau_\lambda^U\right) \partial f_0 / \partial T \quad (15)$$

The different scattering rates or lifetimes in Equations (13)-(15) have the following relations:

$$1/\tau_\lambda^C = 1/\tau_\lambda^R + 1/\tau_\lambda^N \quad (16)$$

$$1/\tau_\lambda^R = 1/\tau_\lambda^U + 1/\tau_\lambda^I \quad (17)$$

$$1/\tau_\lambda^U = B_U \omega^{\alpha_U} T^{\beta_U} e^{-\theta_D/3T} \quad (18)$$

$$1/\tau_\lambda^N = B_N \omega^{\alpha_N} T^{\beta_N} \quad (19)$$

$$1/\tau_\lambda^I = A\omega^4 \quad (20)$$

where x means the direction of temperature gradient, the superscripts C, R, U, N and I respectively mean the total scattering events, resistive scattering events, Umklapp

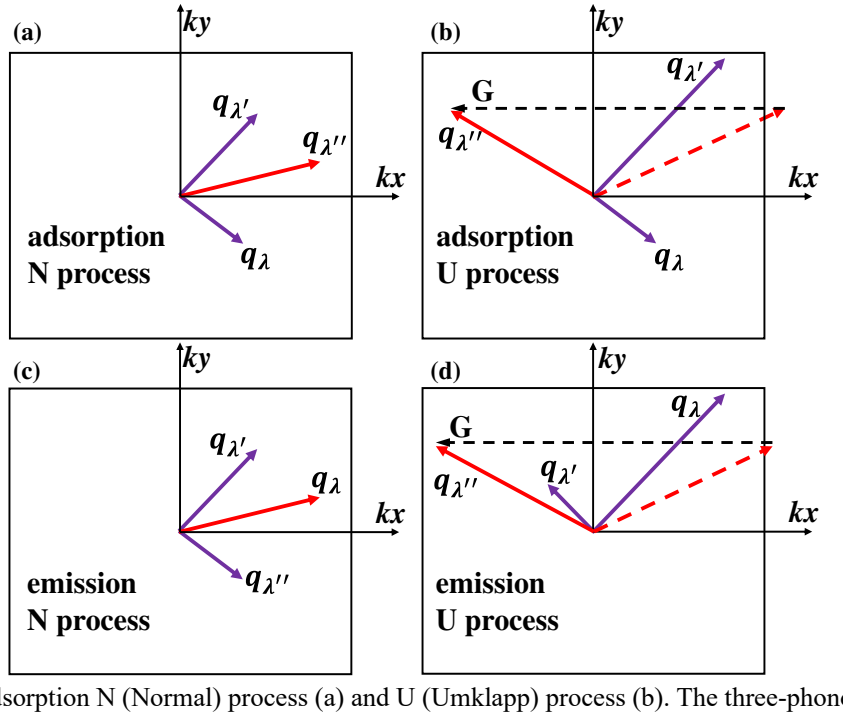

Fig. 1 The three-phonon adsorption N (Normal) process (a) and U (Umklapp) process (b). The three-phonon emission N process (c) and U process (d). The rectangles in black color mean the first Brillouin zone. The dash line means the reciprocal lattice vector G.

scattering events, Normal scattering events and impurity scattering events. Note that R scatterings include U and I scatterings. The parameters A, B_N, B_U, α_N, α_U, β_N, β_U and θ_D in those scatterings are obtained by fitting the temperature dependent thermal conductivity k_{total} from first-principles calculation based on Equations (1)-(4). All the other symbols in Equations (11)-(20) have the same physical meanings as above equations. Here, the width and length effects on phonon transport behavior are also discussed, thus the R scattering rates in Equation (17) should also include the phonon-boundary scattering rates from two boundaries along the width direction and phonon-end scattering rates from two ends along the length direction:[2,34]

$$1/\tau_\lambda^R = 1/\tau_\lambda^U + 1/\tau_\lambda^I + 1/\tau_\lambda^W + 1/\tau_\lambda^L \quad (21)$$

$$1/\tau_\lambda^W = \frac{v_\lambda^\perp F_\lambda^p}{W[1-F_\lambda^p \Lambda_{int,\lambda}^\perp/W]} \quad (22)$$

$$F_\lambda^p = \frac{(1-p_\lambda)[1-\exp(-W/\Lambda_{int,\lambda}^\perp)]}{1-p_\lambda \exp(-W/\Lambda_{int,\lambda}^\perp)} \quad (23)$$

$$1/\tau_\lambda^L = \frac{v_{\lambda x}}{L[1-\exp(-L/\Lambda_{int,\lambda}^x)]} \quad (24)$$

$$\Lambda_{int,\lambda} = v_\lambda \tau_{int,\lambda} \quad (25)$$

$$1/\tau_{int,\lambda} = 1/\tau_\lambda^U + 1/\tau_\lambda^I + 1/\tau_\lambda^N \quad (26)$$

where x means the direction of temperature gradient as above, $\perp$ means the direction perpendicular to x, p is specularity parameter, Λ_{int} is the phonon mean free path due to all intrinsic scattering events including N, U and I scatterings.

3. Results and Discussions

The phonon dispersions within 0-5 THz at different thicknesses along Γ-Y direction of Brillouin zone, *i.e.* a-axis direction of TiS_3 unit cell, are shown in Figs. 2(a)-(c). The direction of temperature gradient is set along a-axis direction as well. Based on those profiles, ZA modes (the lowest phonon branch) have the quadratic dependence on wavevector. In graphene, the hydrodynamic phonon transport is mainly caused by ZA modes, having the similar quadratic shape.[3,35,36] Correspondingly, TiS_3 may also have the hydrodynamic phonon transport. There are two reasons why ZA modes in layered materials contribute significantly to hydrodynamic phonon transport. One is the quadratic shape. Compared to TA and LA phonons, such quadratic shape makes much larger number of ZA phonons at certain temperature. The other is the large anharmonicity,[37-39] which makes N scattering rates much larger than R scattering rates. Thus, the hydrodynamic phonon transport may be a common phenomenon in layered materials. For example, through first-principles calculation, Cepellotti *et al.*[40] recently showed that in layered materials graphene, graphane, fluorographene, boron nitride and molybdenum disulphide, N scattering rates are larger than U scattering rates especially at low temperature.

As discussed above and shown in Ref. 3, the linear dependence of normalized deviation of phonon distribution $\bar{f}'$ on wavevector is a strong indicator of macroscopic drift motion of phonons and the slope of this dependence is the value of drift velocity. The Equation (9) is applied to calculate $\bar{f}'$, where the direction of temperature gradient is chosen along a-axis direction and F is obtained from ShengBTE package. The calculated $\bar{f}'$ at 100 K along q_a direction, *i.e.* Γ-Y direction in Figs. 2(a)-(c), with different thicknesses clearly

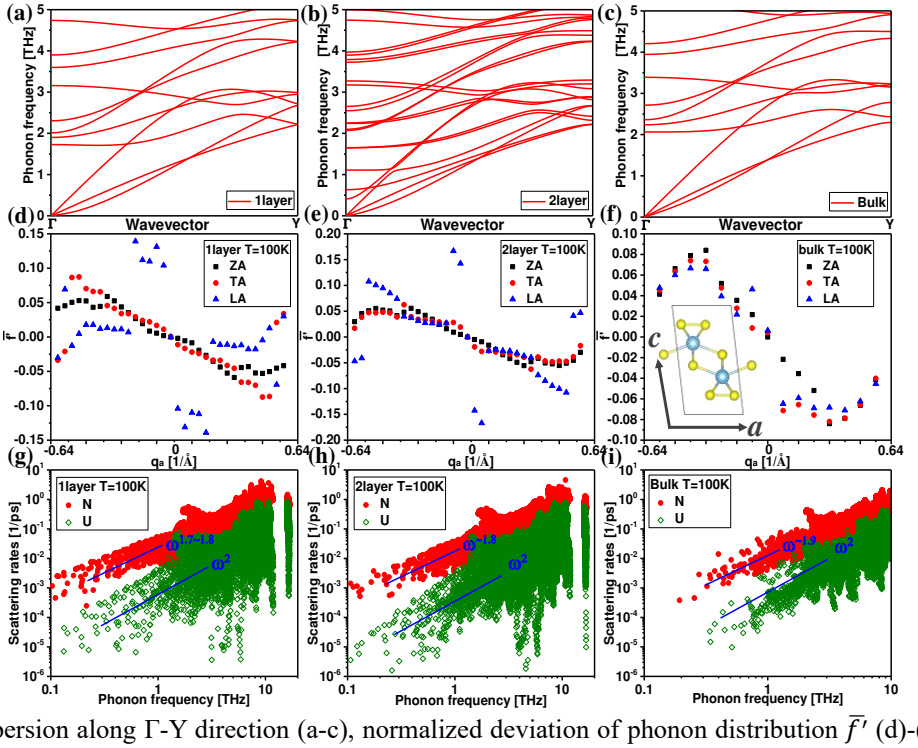

Fig. 2 The phonon dispersion along Γ-Y direction (a-c), normalized deviation of phonon distribution $\bar{f}'$ (d)-(f) as well as N and U scattering rates (g)-(i). The inset in (f) shows the unit cell of TiS_3. The linear dependences of $\bar{f}'$ on wavevector ((d)-(f)) indicate the hydrodynamic phonon transport. The direction of heat flux or the direction of temperature gradient is along a axis (Γ-Y). The dependences of N and U scattering rates on frequency shown in blue color ((g)-(i)) are from Callaway fitting.

shows a linear dependence on wavevector. And the slopes for ZA, TA and LA modes are exactly same regardless of phonon wavevector and phonon polarization. From the value of slope and equation (6), the drift velocity u of monolayer TiS_3 is extracted. The extracted value of u is 1954 m/s at 50 K and decreases to 241 m/s at 100 K under a temperature gradient 10^7 K/m. Such large decrease may be the reason why hydrodynamic phonon transport is not observable at high temperature. For the decrease of drift velocity, the reason is not clear and it thus needs more work. We infer that with the temperature increasing, the phonon collision frequency increases, *i.e.* the phonon collision time decreases, which causes the decrease of drift velocity. Based on the constant drift velocity at 50 K and 100 K, there exists the macroscopic motion of phonons, indicating the existence of hydrodynamic phonon transport. As pointed in Ref.,[3] if there is no macroscopic motion of phonons, $\bar{f}'$ has no dependence on phonon modes. The non-linear dependences at large wavevector regions of Figs. 2(d)-(f), *i.e.* near the boundary of Brillouin Zone, indicate that the hydrodynamic phonon transport is mainly caused by low-frequency phonons. This is reasonable since high-frequency phonons near the boundary of Brillouin Zone have large wavevector and are involved in Umklapp (resistive) scattering process (Figs. 1(b) and (d)) more easily.

The macroscopic drift motion of phonons can be explained by the fact that there exist much stronger N scattering rates than R scattering rates shown in Figs. 2(g)-(i), which is another indicator of hydrodynamic phonon transport. At 100 K, the N scattering rates of TiS_3 at different thicknesses are about 10-100 times larger than U scattering rates. During N scattering process phonons approach the same drifty velocity by exchanging their momenta and obeys the displaced phonon distribution in Equation (5), while in U scattering process phonons relax to the equilibrium phonon distribution f_0 by destroying their momenta. Under a temperature gradient, such stronger N scattering rates in TiS_3 make phonon distribution displaced (Figs. 2(d)-(f)) and then most phonons have the same drift velocity, *i.e.* macroscopic drift motion of phonons. Similar results are shown on graphene[3] and graphite[4] in previous calculations.

As discussed above, the hydrodynamic phonon transport in TiS_3 is explored based on the linearized phonon Boltzmann transport equation as well as first-principles calculation. In the next part, the improved Callaway model[19] is further applied to investigate the hydrodynamic transport. Since there lacks enough experimental data of temperature dependent thermal conductivity, the parameters (Equations (18)-(20)) in the improved Callaway model are fitted through the data from first-principles calculation. In order to make the parameters realiable, before fitting the model, some parameters are determined based on the frequency dependent scattering rates shown in Figs. 2(g)-(i) from first-principles calculation. By fitting the data of U scattering rates, we find $1/\tau_\lambda^U$ have a quadratic dependence on ω. Thus, $\alpha_U = 2$ is chosen in Equation (18). Many previous studies also applied $\alpha_U = 2$ to describe the U scattering process and obtained satisfactory results.[2] For the value of α_N in Equation (19), different studies adopt different data. For example, Torres *et al.* adopted $\alpha_N = 2$ to describe N scattering rates in silicon rod,[5] while Majee *et al.* adopted $\alpha_N = 1$ in graphene ribbon.[2] Furthermore, the first-principles calculation in graphene[3] and graphite[4] even show that N scattering rates have a weak dependence on ω, i.e. $\alpha_N = 0$. Different values of α_N indicates that the dependence of N scattering rates on ω is different in different materials and the value of α_N is not a constant for all materials. α_N in a certain material therefore is determined by its intrinsic scattering environment, *i.e.* second-order and third-order force constants. Thus, in our work, α_N is determined by fitting the frequency dependent N scattering rates from first-principles calculation, which is obtained based on second-order and third-order force constants. For the temperature related parameters of β_N and β_U, different values are tried and $\beta_N = 1$ and $\beta_U = 1$ give the best fitting results of temperature dependent thermal conductivity (Fig. 3(a)).

After all the parameters are obtained, the resistive thermal conductivity K_C and non-resistive thermal conductivity K_N can be calculated separately from the improved Callaway model. By comparing the magnitudes of K_N and K_C, the thickness and temperature dependent hydrodynamic phonon transport are discussed. For the thickness dependent phonon transport behavior, K_N decreases while K_C increases monotonously with the thickness increasing from 1 layer to 3 layers (Figs. 3(b)-(d)) among the whole temperature range 80-700 K. So, hydrodynamic phonon transport becomes weakened with the thickness increasing. That is reasonable since the interlayer coupling strength can enhance the resistive scattering.[11] With the thickness approaches 3 layers, K_N is close to K_C at temperature larger than 200 K, indicating the disappearance of the observed hydrodynamic transport. Due to the computational cost, the phonon transport in thicker TiS_3 is not calculated. By comparing the profiles in Figs. 3(a) and (d), the phonon transport behavior in bulk structure is similar to 3 layers. Further analysis based on our calculation shows that the hydrodynamic phonon transport is more obvious in bulk structure than that in 3 layers. We will discuss it later. Thus, the hydrodynamic phonon transport has a non-monotonic dependence on thickness. For the temperature dependent phonon transport behavior, both K_N and K_C at all calculated thicknesses increase monotonously with the temperature decreasing from 700 K to 80 K. And K_N shows a more obvious increase than K_C. Thus, at low temperature, the hydrodynamic phonon transport is easier to be observed. By comparing K_N and K_C profiles in Fig. 3, hydrodynamic phonon transport is observable around 100 K for all thicknesses, since K_N is much larger than K_C. While at 300 K, the hydrodynamic phonon transport is not dominant and unobservable in 3 layers and bulk TiS_3.

In real experiment, the width or length of the sample are not infinite. Thus, the effects of width and length on phonon

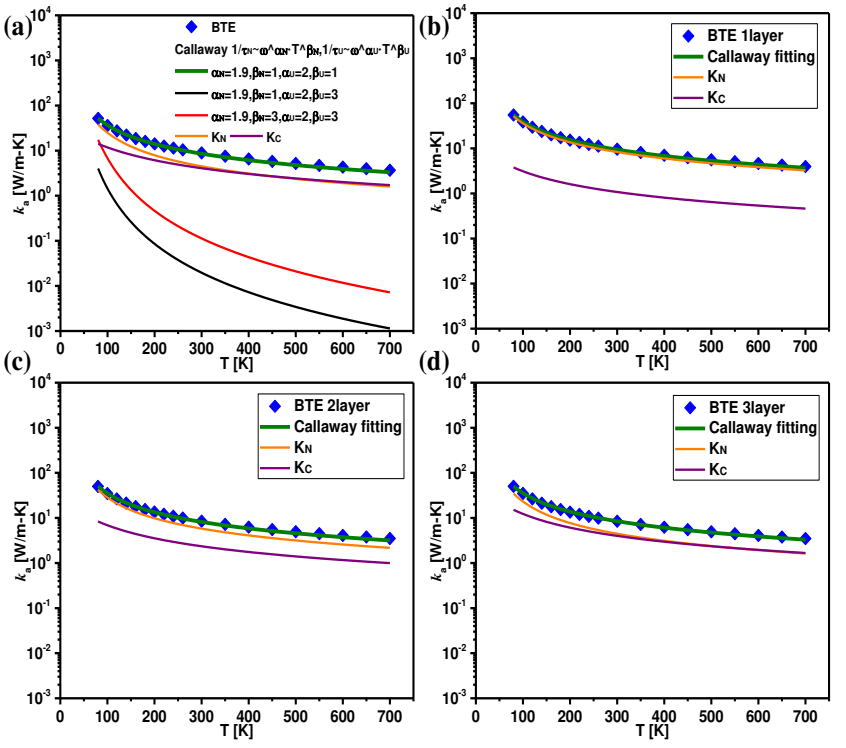

Fig. 3 The temperature dependent thermal conductivity along *a*-axis direction for bulk (a), 1 layer (b), 2 layers (c) and 3 layers (d) TiS_3. The blue diamond points mean the data from first-principles calculation. The olive lines (k_{total}), orange lines (K_N) and purple lines (K_C) respectively mean the total thermal conductivity, N-drift term (non-resistive) thermal conductivity and Debye term (resistive) thermal conductivity from the Callaway model fitting based on equations (10)-(20). For bulk TiS_3, different values of β_N and β_U are chosen during the fitting, and β_N = 1and β_U =1 give the best fitting results.

transport behavior are calculated and discussed. The scattering rates caused by two boundaries of width and caused by two ends of length are described by $1/\tau_\lambda^W$ in Equation (22) and $1/\tau_\lambda^L$ in Equation (24) respectively. The specularity parameter p of boundary in Equation (23) is chosen as 0.5, representing partially specular and partially diffusive boundary scattering. The calculation results in Fig. 4 show that at short width, K_C is larger than K_N. That is reasonable since short width has

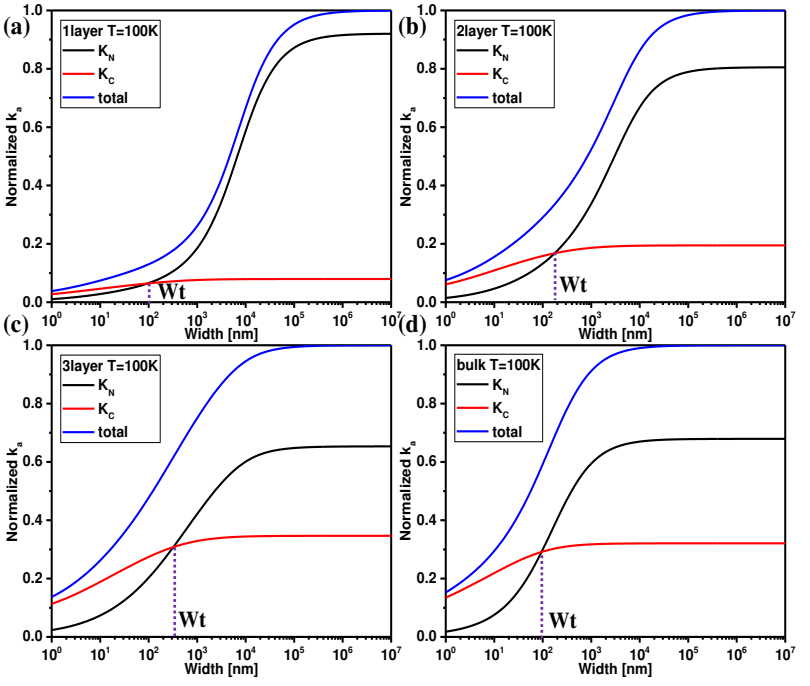

Fig. 4 The width dependent normalized thermal conductivity along *a* axis at 100 K in 1 layer (a), 2 layers (b), 3 layers (c) and bulk TiS_3 (d). The blue lines, black lines and red lines respectively mean k_{total}, K_N and K_C. The dashed line means the value of W_t, which represents the transition of relative relation between K_N and K_C.

larger resistive phonon-boundary scatterings. With the width increasing, both K_N and K_C increases monotonously. However, K_N increases more obviously than K_C. Thus, at a certain width defined as transition width W_t here, the value of K_N exceeds that of K_C. And the value of W_t is dependent on thickness. As the thickness increases from 1 layer to 3 layers, W_t increases from 100 nm to 300 nm monotonously. The larger value of W_t at larger thickness means stronger R scattering at larger thickness, which is reasonable since the interlayer coupling scatterings are resistive and increase with thickness. Interestingly, W_t of bulk structure is smaller than that of 3 layers, indicating a non-monotonic dependence of W_t on thickness. Similar non-monotonic dependence of thermal conductivity on thickness was observed recently in van der Waals stacked materials.[16,18] The reason here is contributed to the competition between phonon-phonon scattering and phonon-boundary scattering induced by phonon confinement effects as well.[17] As the thickness is small and phonon-phonon scatterings are dominant, W_t has a positive dependence on thickness due to the increase of resistive interlayer phonon-phonon scattering; while as the thickness is large enough to make phonon-boundary scatterings dominant, W_t has a negative dependence on thickness due to the decrease of resistive phonon-boundary scattering. Thus, the transition width W_t between K_N and K_C has an interesting and non-monotonic dependence on thickness, indicating a non-monotonic dependence of hydrodynamic phonon transport on thickness in layered materials. It should be noted that the value of W_t here is based on p of 0.5, *i.e.* partially specular and partially diffusive boundary scattering. By decreasing the value of p, *i.e.* the increase of diffusive boundary scattering, the hydrodynamic phonon transport is suppressed and the transition width W_t increases.

The length effects on phonon transport behavior are similar to the width effects as shown in Fig. 5. At short length, K_C is larger than K_N, which is caused by the resistive phonon-end scatterings. With the length increasing, both K_N and K_C increases and K_N shows a more obvious increase than K_C. Thus, at a certain length defined as transition length L_t, the value of K_N exceeds that of K_C. L_t has a similarly non-monotonic dependence on thickness as W_t and the reason is similarly attributed to the competition between phonon-phonon scatterings and phonon-end scatterings. By increasing the width, L_t is shown to have a negative dependence on W. The reason is because with W increasing, the resistive phonon-boundary scatterings decrease and then L_t decreases.

4. Summary

The thickness dependent hydrodynamic phonon transport in layered TiS_3 is investigated by first-principles calculation and improved Callaway model. From the picture of linearized phonon Boltzmann transport based on first-principles calculation, the phonon distribution at 100 K of TiS_3 is well displaced with a constant drift velocity regardless of phonon wavevector and phonon polarization, indicating the existence of the hydrodynamic phonon transport. The much larger N

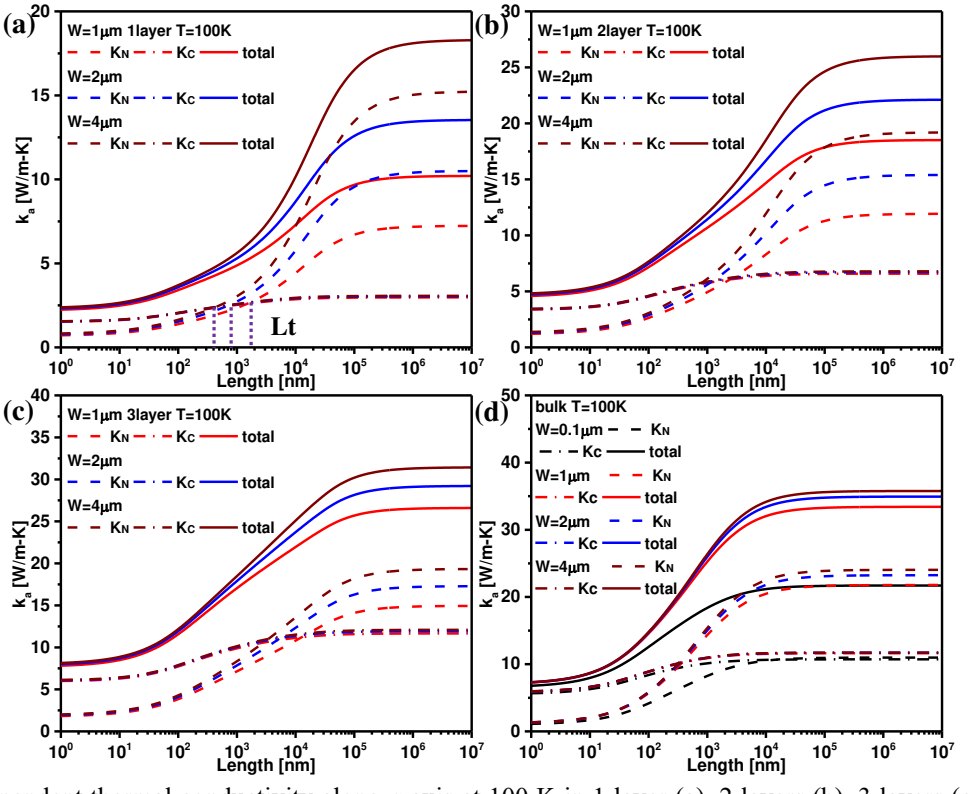

Fig. 5 The length dependent thermal conductivity along *a* axis at 100 K in 1 layer (a), 2 layers (b), 3 layers (c) and bulk TiS_3 (d). Three different widths of W = 1 μm (red lines), 2 μm (blue lines) and 4 μm (wine lines) are calculated. The solid lines, dashed lines and dashed dot lines mean k_{total}, K_N and K_C respectively. The dashed line means the value of L_t, which represents the transition of relative relation between K_N and K_C. From the dashed purple lines in (a), with W increasing L_t decreases monotonously.

scattering rates than U scattering rates at 100 K can explain the constant drift velocity. From the improved Callaway model, the non-resistive N-drift thermal conductivity K_N is much larger than the resistive Debye thermal conductivity K_C at 100 K, another indicator of the hydrodynamic phonon transport. With the thickness increasing from 1 layer to 3 layers, the value of K_C approach K_N and even exceeds K_N at 3 layers with temperature larger than 200 K, which is caused by the increase of resistive interlayer coupling scatterings. At short width, K_N is smaller than K_C, while with the width increasing, K_N exceeds K_C at a certain value named as W_t. The value has an interesting and non-monotonic dependence on thickness due to the competition between phonon-phonon scatterings and phonon-boundary scatterings. The effects of length on phonon transport behavior are similar to those of width. The results here can provide physical insights into the thickness dependent hydrodynamic phonon transport in layered materials.

Acknowledgements

This work was supported by the Natural Science Foundation of Jiangsu Province (Grant no. BK20210565) and Jiangsu Specially-Appointed Professor Program (Grant no. 164080H00230). This work was also supported by the National Natural Science Foundation of China (No. 51878356) and the open research fund of Jiangsu Key Laboratory for Design and Manufacture of Micro-Nano Biomedical Instruments, Southeast University (No. KF202010) as well. The authors thank the Big Data Center of Southeast University and Jiangsu Key Laboratory for Numerical Simulation of Large Scale Complex Systems for providing the facility support on numerical calculations in this work.

Conflict of Interest

There is no conflict of interest.

Supporting Information

Not Applicable.

References

[1] L. Lindsay, *Nanosc. Microsc. Therm.,* 2016, **20**, 67-84.
[2] A. K. Majee and Z. Aksamija, *Phys. Rev. B,* 2016, **93**, 235423.
[3] S. Lee, D. Broido, K. Esfarjani and G. Chen, *Nat. Commun.,* 2015, **6**, 6290.
[4] Z. W. Ding, J. W. Zhou, B. Song, V. Chiloyan, M. D. Li, T. H. Liu and G. Chen, *Nano Lett.,* 2018, **18**, 638-649.
[5] P. Torres, A. Torello, J. Bafaluy, J. Camacho, X. Cartoixa and F. X. Alvarez, *Phys Rev. B.,* 2017, **95**, 165407.
[6] S. Lee and L. Lindsay, *Phys. Rev. B,* 2017, **95**, 184304.
[7] Y. Machida, A. Subedi, K. Akiba, A. Miyake, M. Tokunaga, Y. Akahama, K. Izawa and K. Behnia, *Sci. Adv.,* 2018, **4**, eaat3374.
[8] Y. Machida, N. Matsumoto, T. Isono and K. Behnia, *Science,* 2020, **367**, 309.
[9] X. Li and S. Lee, *Phys. Rev. B,* 2019, **99**, 085202.
[10] Y. Cheng, X. Wu, Z. J. Zhang, Y. Sun, Y. S. Zhao, Y. Y. Zhang and G. Zhang, *Nanoscale,* 2021, **13**, 1425-1442.
[11] L. Shi, *Science,* 2019, **364**, 332-333.
[12] C. H. Liu, P. Lu, W. Chen, Y. Zhao and Y. F. Chen, *Phys. Chem. Chem. Phys.,* 2021, doi: 10.1039/d1cp02328d.
[13] L. Mezhov-Deglin, *Sov. Phys. JETP*, 1966, **22**, 47.
[14] H. E. Jackson, C. T. Walker and T. F. McNelly, *Phys. Rev. Lett.,* 1970, **25**, 26-28.
[15] P. K. Schelling and R. Keblinski, *Phys. Rev. B,* 2003, **68**, 035425.
[16] L. Yang, Y. Tao, Y. L. Zhu, M. Akter, K. Wang, Z. L. Pan, Y. Zhao, Q. Zhang, Y. Q. Xu, R. K. Chen, T. T. Xu, Y. Chen, Z. Mao, D. Li, *Nat. Nanotechnol.,* 2021, **16**, 764.
[17] B. Fu, K. D. Parrish, H. Y. Kim, G. H. Tang and A. J. H. McGaughey, *Phys. Rev. B,* 2020, **101**, 045417.
[18] C. H. Liu, P. Lu, D. Li, Y. Zhao and M. Hao, Thickness dependent and anisotropic in-plane thermal transport in layered titanium trisulphide: First-principles calculation.
[19] P. B. Allen, *Phys. Rev. B,* 2013, **88**, 144302.
[20] R. A. Guyer and J. A. Krumhansl, *Phys. Rev.*, 1966, **148**, 778-788.
[21] P. Torres, A. Ziabari, A. Torello, J. Bafaluy, J. Camacho, X. Cartoixa, A. Shakouri and F. X. Alvarez, *Phys. Rev. Mater.,* 2018, **2**, 076001.
[22] A. Sellitto, F. X. Alvarez and D. Jou, *Int. J. Heat. Mass. Tran.,* 2012, **55**, 3114-3120.
[23] J. O. Island, M. Barawi, R. Biele, A. Almazan, J. M. Clamagirand, J. R. Ares, C. Sanchez, H. S. J. van der Zant, J. V. Alvarez, R. D'Agosta, I. J. Ferrer, and A. C. Gomez, *Adv. Mater.,* 2015, **27**, 2595-2601.
[24] A. Hayashi, T. Matsuyama, A. Sakuda and M. Tatsumisago, *Chem. Lett.,* 2012, **41**, 886-888.
[25] J. Wu, D. Wang, H. Liu, W. M. Lau and L. M. Liu, *Rsc. Adv.,* 2015, **5**, 21455-21463.
[26] G. Sun, Z. X. Wei, N. Chen, G. Chen, C. Z. Wang and F. Du, *Chem. Eng. J.,* 2020, **388**, 124305.
[27] A. Togo and I. Tanaka, *Scripta. Mater.*, 2015, **108**, 1-5.
[28] W. Li, J. Carrete, N. A. Katcho and N. Mingo, *Comput. Phys. Commun.,* 2014, **185**, 1747-1758.
[29] C. H. Liu, P. Lu, Z. Z. Gu, J. K. Yang and Y. F. Chen, *J. Phys. Chem. C,* 2020, **124**, 26144-26152.
[30] C. H. Liu, Y. F. Chen and C. Dames, *Phys. Rev. Appl.,* 2019, **11**, 044002.
[31] L. Lindsay and D. A. Broido, *J. Phys-Condens. Mat.,* 2008, **20**, 165209.
[32] A. Ward, D. A. Broido, D. A. Stewart and G. Deinzer, *Phys. Rev. B,* 2009, **80**, 125203.
[33] P. G. Klemens, *Handbuch der Physik*, 1956, **14**, 198-281.
[34] Z. Aksamija and I. Knezevic, *Phys. Rev. B,* 2012, **86**, 165246.
[35] T. L. Feng and X. L. Ruan, *Phys. Rev. B,* 2018, **97**, 045202.
[36] X. K. Gu, Z. Y. Fan, H. Bao and C. Y. Zhao, *Phys. Rev. B,* 2019, **100**, 064306.
[37] Y. Q. Cai, Q. Q. Ke, G. Zhang, Y. P. Feng, V. B. Shenoy and Y. W. Zhang, *Adv. Funct. Mater.,* 2015, **25**, 2230-2236.
[38] S. Lee, S. H. Kang and Y. K. Kwon, *Sci. Rep.,* 2019, **9**, 5149.

[39] R. Ramirez and C. P. Herrero, *Phys. Rev. B,* 2020, **101**, 235436.
[40] A. Cepellotti, G. Fugallo, L. Paulatto, M. Lazzeri, F. Mauri and N. Marzari, *Nat. Commun.,* 2015, **6**, 6400.

Author information

Chenhan Liu *received his Ph.D. degree in 2019 from Southeast University, China. During 2016-2018, he went to the University of California, Berkeley to study a joint Ph.D. program. From 2020, he joined the Nanjing Normal University as an assistant professor in School of Energy and Mechanical Engineering. His group currently focuses on nanoscale heat transfer, interfacial thermal transport, thermal control device, thermal management of thermoelectric materials, electrocaloric cooling based on ferroelectric materials and machine learning of thermal science.*

Chao Wu *received her Bachelor's degree in 2017 from Northeast Agricultural University, China. From 2017, she joined the Southeast University as a Ph.D. candidate in school of mechanical engineering. Her research focuses on the measurement and the first-principles calculation of thermal and electric properties of nanowires.*

Ping Lu *received his B.E. degree from Nanjing Tech University in 1990 and Ph.D. degree from Southeast University in 2002. He is full professor and dean of the School of Energy and Mechanical Engineering at the Nanjing Normal University, where he leads the carbon-based energy thermochemical conversion and utilization laboratory. His research activity spans energy technology to environmental engineering. His main research interests include coal combustion and its emissions control; biomass thermochemical conversion, solid waste treatment and numerical simulation.*

Yunshan Zhao *received his B.S. from Shandong University in 2013 and Ph.D. from National University of Singapore in 2017. He worked as Research Fellow in National University of Singapore until 2020. He then joined Nanjing Normal University as a full professor. Prof Zhao's group currently focuses on nanoscale energy transfer in nanostructured materials, such as phonon thermal transport in low dimensional materials and phonon & electron engineering for TE applications as well as electronics of two-dimensional materials.*

